Neuromechanical Coupling is Reflected in the Spatial Organization of the Spinal Motoneuron Pools

Authors: Rachel I. Taitano[1], Sergiy Yakovenko[1,2], and Valeriya Gritsenko[1,2]
Affiliations:
[1] Department of Neuroscience, West Virginia University
2 Department of Human Performance, West Virginia University

Abstract

The anatomy of muscles is complex, so that a given movement can result from the activity of multiple muscle combinations, a concept termed redundancy. The central nervous system must resolve this redundancy to produce coordinated and efficient motion. One proposed mechanism that simplifies motor control is through the neural embedding of musculoskeletal dynamics. We have shown previously that the musculoskeletal anatomy of the upper extremity is organized in functional agonistic and antagonistic groups through mechanical coupling. However, it remains unknown if the neural anatomy of the spinal motoneuron pools somatotopically embeds this musculoskeletal anatomy. Here, we develop a three-dimensional model of the macaque cervical spinal cord and a corresponding OpenSim model of the upper extremity to characterize the structure-function relationship of spinal motoneurons innervating upper limb musculature. We hypothesize that the motoneuron pools of agonistic muscles that perform a coordinated action are located closer together in the spinal cord compared to antagonistic muscles. We used the spinal cord model to quantify the spatial relationship between motoneuron pools, and we used the OpenSim model to quantify the functional relationship between muscles. We used a hierarchical clustering analysis compare the structural and functional relationships. We found that the spatial organization of motoneuron pools in the spinal cord broadly mimics the anatomical relationships between muscle lengths and moment arms. Furthermore, within the same segment, the motoneurons innervating synergistic muscles were located closer to each other than to the motoneurons innervating antagonistic muscles, while across segments the motoneurons innervating specific antagonistic groups of muscles were colocalized. These results suggest that the mechanical coupling of the musculoskeletal system is embedded in the spinal cord anatomy underlying the modular organization of the neural motor control system.

Introduction

The primary role of the nervous system is to generate adaptable and complex movement (Wolpert 2011). The large repertoire and dexterity of human movement relies on the musculoskeletal complexity and sophisticated neural control mechanisms. With such complexity,

redundancy is inevitable, which means that multiple combinations of muscles with variable activation patterns may be recruited by multiple neural circuits to perform the same action (Bernstein 1990). The solution to the redundancy problem lies in the neural embedding of musculoskeletal dynamics, the idea exemplified by internal models (Angelaki et al. 2004; Kawato 1999; McNamee and Wolpert 2019). An analogy of this idea is the use of plane dynamics within the autopilot algorithm. These embedded models of the musculoskeletal system can be used to plan forward neural commands and to predict expected differences in sensory feedback. They are usually associated with the higher levels of the neural hierarchy, such as in the circuits of the neocortex or cerebellum. However, is it possible for the spinal cord to embed musculoskeletal dynamics?

The spinal motor system is through to have a modular organization (for review see (Tresch et al. 2002). In this concept, muscles are controlled in groups activated by few common signals (d'Avella et al. 2003) and supported by neuromechanical interactions and spinal reflexes (Bizzi and Cheung 2013). We set out to evaluate the feasibility of the neural anatomy of spinal motoneuron (MN) pools to support such modularity. In an earlier study we have shown that muscles can be objectively grouped into functional units of agonists and antagonists using just muscle anatomy (Gritsenko et al. 2016). We propose that these musculoskeletal functional units are reflected in the spinal cord anatomy. Specifically, we hypothesize that the MN pools innervating agonistic muscles are located close together in the ventral horn of the spinal cord grey matter, while the MN pools innervating antagonists are spatially separated from each other. This arrangement can support the modular organization of spinal motor systems by creating the neuromuscular processing units that are optimally co-localized to receive common descending inputs and share sensory feedback with minimal delays. To test this idea, we have built a three-dimensional model of the anatomical locations of spinal MN pools in the thoracic and cervical segments of the spinal cord using published data (Jenny and Inukai 1983). We then used hierarchal clustering to quantify the spatial relationship between the MN pools and to compare it to the functional relationships between muscles they innervate.

Materials & Methods

<u>Spinal Cord Motoneuron Model</u>

Locations of motoneuronal cell bodies innervating macaque forelimb muscles were acquired from a previous study utilizing retrograde transport of horseradish peroxidase in 10 *M. mulatta* and 4 *M. fascicularis* monkeys (Jenny and Inukai 1983). Images of spinal cord sections C5 through T1, were divided into rostral and caudal segments, scanned, and digitized using Adobe Illustrator (Adobe Inc). Metadata from these images was then used to generate a 3D model of spinal MNs in Matlab (Mathworks), similar to our previous work (Yakovenko et al. 2002). One set of grey matter outlines (*M. fascicularis* subject 79-1 from (Jenny and Inukai 1983)) was selected to be used in our model to account for differences in animal size and anatomical variability across subjects. Each grey matter outline from the remaining subjects was scaled to match the

dimensions of the selected sections along the anterior/posterior and medial/lateral axes. MN coordinates obtained from other subjects were then also normalized to the selected outlines based on their relative position in the spinal cord grey matter. The relative perpendicular distances from each coordinate to the original grey matter outline along the anterior/posterior and medial/lateral axes were scaled using the same ratios used to scale each grey matter outline to those selected. Anatomical sizes of spinal segments of monkeys from an atlas (Watson et al. 2022) were used to scale the rostral/caudal coordinates relative to the anterior/posterior and medial/lateral coordinates for all MNs and grey matter outlines.

Due to the resolution of images included in the original study, digital extraction of MN coordinates based on a pixel by pixel analysis led to differences in the number of MNs reported in the original data compared to those extracted from the digitized sections. As such, MN coordinates were resampled to match the rostro-caudal distributions reported in the original data for each spinal cord section. Briefly, if our analysis included more MNs that originally reported, then indices of MNs for each spinal cord section were randomly selected for removal. Conversely, if the original paper reported more MNs than were identified when the images were scanned and digitized, MN coordinates were randomly added to the model. The mean, range, and standard deviation of MN coordinates within each level, as well as the density of MNs across levels were held constant. MN pools were originally modeled localized to the side for which the data was originally obtained, then all MN coordinates were reflected to one side for all analyses and visualizations (Fig. 1).

OpenSim Upper Extremity Models

OpenSim (version 4.1, Stanford University, Stanford, CA, USA) was utilized to model the musculoskeletal anatomy of both the macaque and human right upper limb. Utilization of this software allows for the study of musculoskeletal interactions in a non-invasive manner, over a range of user-defined conditions. The macaque OpenSim model developed by Chan and Moran (Chan and Moran 2006) was modified to increase the number of muscles available for comparison with the spinal cord MN data. The following forelimb muscles have been added or modified based on anatomical data (Berringer et al. 1968): adductor pollicis, dorsal interossei, extensor digitorum, extensor pollicis longus, flexor digitorum profundus, flexor digitorum superficialis, lumbricals, and ventral interossei (Fig. 2A). Muscles with multiple heads and/or points of insertion were modeled as separate units. For example, the biceps brachii was modeled as two muscles, the biceps long head and the biceps short head. Similarly, the extensor digitorum was modeled as 4 muscles, sharing a similar origin, but inserting on each corresponding distal phalange of digits 2-5. Addition of these muscles allowed for modeling of the carpometacarpal (CMC), metacarpophalangeal (MCP), and interphalangeal (IP) joints of the digits, increasing the total degrees of freedom (DOFs) in the macaque model to 27. These added DOFs were necessary to accurately model changes in muscle lengths across different postures. The carpometacarpal joint of the thumb and the metacarpophalangeal joints of digits 2-4 were modeled with 2 DOFs, representing flexion/extension and abduction/adduction around the x- and z-axes, respectively. Interphalangeal joints were modeled as a single DOF representing flexion/extension about the x-axes. Muscle

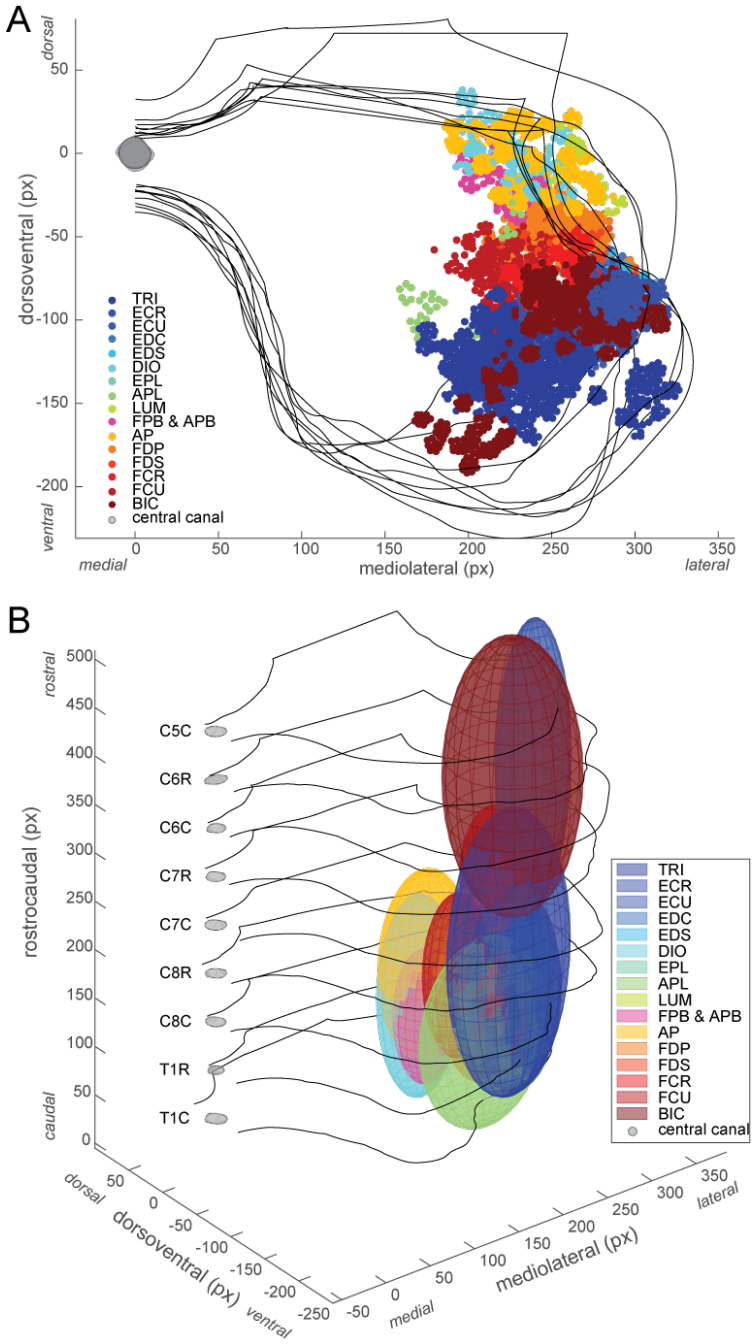

abbreviations used in this study can be found in Table 1.

An OpenSim model of the human arm was used to assess functional differences between macaque and human musculoskeletal anatomy. The original model developed by (Saul et al. 2015) was modified similarly to the macaque model outlined above (Fig. 2B) in a previous study (Gritsenko et al. 2016). The carpometacarpal joint of the thumb was modeled with 2 DOFs, representing flexion/extension and abduction/adduction around the x- and z-axes, respectively. Metacarpophalangeal and interphalangeal joints of digits 2-4 were modeled as a single DOF representing flexion/extension about the x-axes. With the included modifications, there were 23 total DOFs in our human model, similar to the macaque model.

Figure 1. Macaque spinal cord model. Each symbol shows a MN location scaled to a single set of grey matter outlines for spinal segments C5 - T1. Central canal locations are shown as gray circles, used to align the grey matter outlines. Transverse (**A**) and 3D (**B**) view of the macaque spinal cord model.

<u>Hierarchical Clustering Analysis</u>

The relative distances between the center of mass for each pair of MN pools were calculated and hierarchical clustering was applied to quantify their spatial relationship, similar to our previous work (Gritsenko et al. 2016). Musculotendon lengths (i.e., muscle lengths) were calculated for each forelimb posture across the physiological range of motion in the OpenSim model using Matlab. The correlation matrix of muscle lengths across all postures was converted to heterogeneous variance explained (HVE) to emphasize agonistic relationships (Hardesty et al.

2020). Hierarchical clustering was applied to HVE using the linkage function in Matlab to quantify the functional relationships between muscles. Seven different clustering algorithms were considered and the method with the highest cophenetic correlation coefficient was applied to the data. In a comparable manner, moment arms for each muscle in the model were calculated as a second measure of muscle function. Correlation coefficients for moment arms were calculated for each pair of muscles and the hierarchical clustering method used for muscle lengths was applied to these correlation coefficients.

Centers of MN pools were calculated as a center of mass. Distances between the center of mass for each MN group were calculated in Matlab using the distance formula. Relative distances between each center of mass were calculated along all three axes, and again separately along the anterior/posterior plus medial/lateral axes. These two analyses were both included since many neuronal axons travel between spinal cord levels, and we are interested in how MN pools are controlled by supraspinal and feedback mechanisms, thus the rostrocaudal relationships may be of less significance. The same hierarchical clustering function was applied to these distances as to the HVE.

Table 1. Muscle name abbreviations

Abbreviation	Muscle Name		Abbreviation	Muscle Name
ANC	Anconeus		FCU	Flexor carpi ulnaris
AP	Adductor pollicis		FPL	Flexor pollicis longus
APB	Abductor pollicis brevis		FDP	Flexor digitorum profundus
APL	Abductor pollicis longus		FDS	Flexor digitorum superficialis
BIC	Biceps		ISPI	Infraspinatus
BR	Brachialis		LATD	Latissimus dorsi
BRR	Brachioradialis		LUM	Lumbricalis (lateral)
CORBR	Coracobrachialis		PALL	Palmaris longus
DELT	Deltoid		PEC	Pectoralis
DIO	Dorsal interosseous		PQUAD	Pronator quadratus
DOR	Dorsoepitrochlearis		PTER	Pronator teres
ECR	Extensor carpi radialis		SSCAP	Subscapularis
ECU	Extensor carpi ulnaris		SUP	Supinator
ED	Extensor digitorum		SSPI	Supraspinatus
EDM	Extensor digiti minimi		TERMA	Teres major
EDS	Extensor digiti secundi proprius		TERMI	Teres minor
EIND	Extensor indicis		TRI	Triceps

EPL	Extensor pollicis longus		VIO	Ventral interosseous
FCR	Flexor carpi radialis			

Statistical Analysis

Cluster assignments obtained from the locations of MN pools, muscle lengths, and moment arms were compared using the Fowlkes-Mallows index (B_k) to evaluate the similarity between clusters across the different anatomical variables (Fowlkes and Mallows 1983). Briefly, this method is used to compare two hierarchical cluster trees. Each cluster tree is cut to a set height such that there are $k = 2, \ldots, (n - 1)$ clusters for each tree, where n is equal to 16 MN pools included in the spinal cord model. Any combination of two clusters from different trees being compared are then combined into a single matrix containing elements m_{ij} signifying the number of objects in common with the ith cluster of the first tree and j^{th} cluster of the second tree. The following equations describe the calculations of the Fowlkes-Mallows index (B_k) from the number of common members (m_{ij}) for the arbitrary number of clusters.

$$B_k = \frac{T_k}{\sqrt{P_k Q_k}}$$

where

$$T_k = \sum_{i=1}^{k} \sum_{j=1}^{k} {m_{ij}}^2 - n$$

$$P_k = \sum_{i=1}^{k} \left(\sum_{j=1}^{k} m_{ij} \right)^2 - n$$

$$Q_k = \sum_{j=1}^{k} \left(\sum_{i=1}^{k} m_{ij} \right)^2 - n$$

For each k, $0 \leq B_k \leq 1$, where $B_k = 1$ occurs when the clusters in the two trees being compared are equal. Conversely, $B_k = 0$ when the elements of each cluster tree are different between the two trees being compared.

Statistical comparison of clusters obtained from changes in muscle length was evaluated through bootstrapping of MN coordinates and muscle lengths in macaque models. MN coordinates were resampled 1,000 times with replacement and with preservation of data structure, so that the same samples were obtained from each MN pool (Efron and Tibshirani 1994). The muscle lengths were resampled 1,000 times as described in detail in (Gritsenko et al. 2016). Then hierarchal clustering was applied to each bootstrap and 1,000 B_k values were calculated for each cluster

subdivision (i.e., from subdivision into 2 through 8 clusters).

To estimate noise, cluster assignments from hierarchical clustering of MN pools and muscle lengths in the macaque models were randomly permuted 1,000 times and the B_k value was calculated for each bootstrap.

Statistical significance of B_k values obtained from the model was determined using the percentile method (Efron and Tibshirani 1994). The chance of making Type I error (p-value) was estimated as the percentage of when a given B_k value lies in the distribution of noise. The significant alpha was set to 0.007 to correct for multiple comparisons.

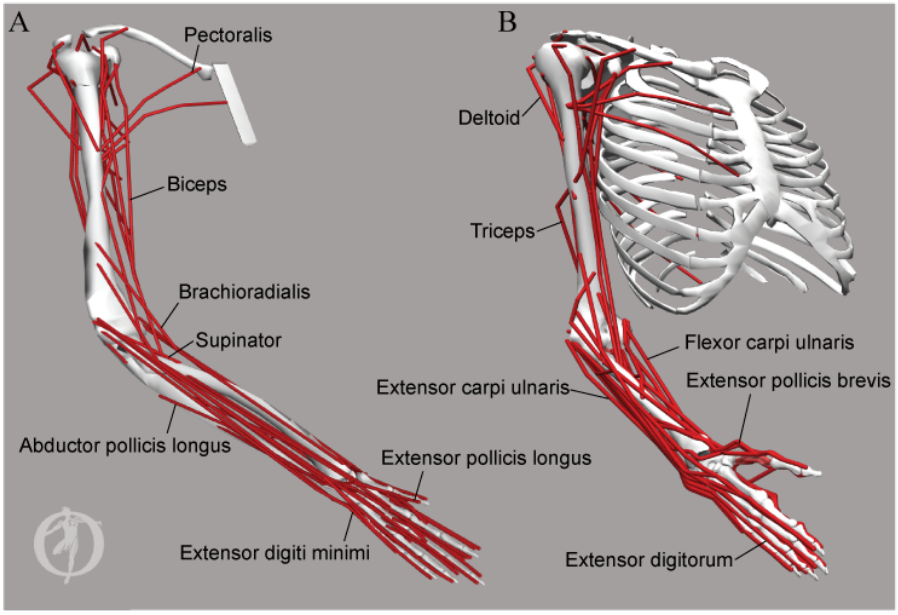

Figure 2. OpenSim musculoskeletal models. **A.** Upper extremity of the macaque modeled with 27 degrees of freedom. **B.** Upper extremity of the human modeled with 23 degrees of freedom.

Results

<u>The anatomy of motoneuron pools in macaque spinal cord</u>

The MN pools for skeletal muscles of the forearm were distributed along multiple segments in macaque spinal cord (Fig. 1B and Fig. 3, dark bars). The MNs innervating more proximal arm muscles, such as the biceps and triceps, were located in the more rostral spinal segments compared to the MNs innervating the intrinsic hand muscles, which were located in the more caudal spinal segments (Fig. 3). The MN pools innervating the wrist muscles (FCR, FCU, ECR) fit in-between. This is similar to the more rostral location of the MNs innervating the proximal muscles of the lower limb in cat lumbar enlargement compared to the distal location of the MNs innervating the distal muscles (Yakovenko et al. 2002). In the human, the rostrocaudal distribution of MN pools is unknown, but it has been estimated based on the spinal segments, from which nerves projecting to upper limb muscles originate (Kendall et al. 1993) (Fig. 3, light bars). Twelve out of 16 MN pools overlap in their rostrocaudal distribution between human estimates and macaque anatomy. The overlapping anteroposterior locations of MN pools innervating some finger muscles (EDC, EDS, EPL, and APL) in the macaque compared to that in the human may underlie the lower-

dimensional functional coupling between muscles of macaque hand suited for less dexterous movements compared to that of the human hand.

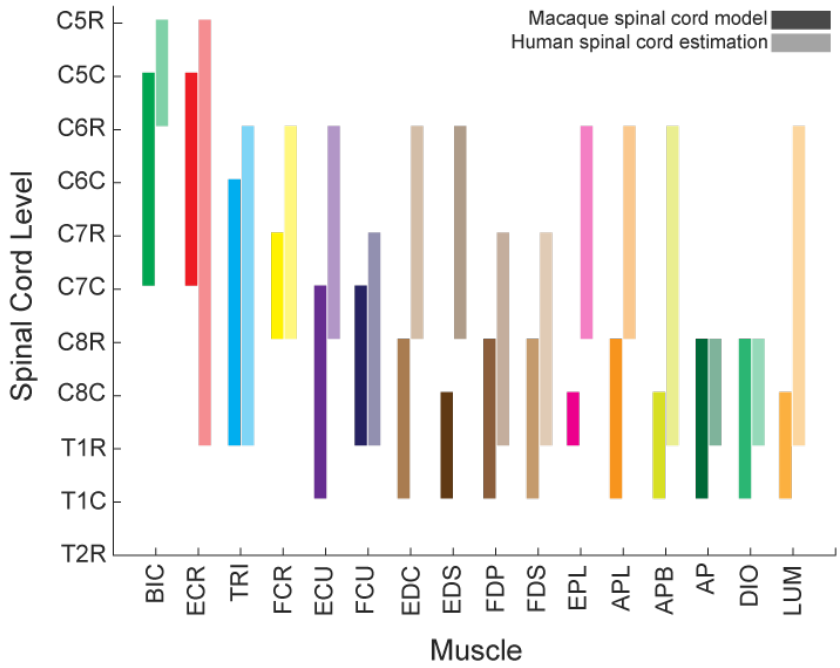

Figure 3. The rostrocaudal distribution of MNs in the macaque vs. human spinal cord. Distribution of MN pools along spinal segments in the macaque model vs. human estimates adapted from Kendall and McCreary (1993). Dark bars represent the levels of motoneuronal cell bodies in the macaque spinal cord model. Light bars indicate the spinal levels that contribute to the formation of nerves innervating the selected muscles.

What are the relationships between the anatomical locations of different MN pools? To answer this question, we applied hierarchical clustering to the relative distances between the centers of MN pools. We found that the MNs innervating some thumb muscles and intrinsic hand muscles (AP, DIO, APB, and LUM) were located closer to each other than to other muscles (Fig. 4A, yellow cluster). Similarly, the MNs innervating extensors of the wrist and fingers and thumb abductor (EPL, APL, EDC, and ECU) were located closer to each other than to other muscles with further subdivision into thumb cluster and extensors of finger and wrist cluster (Fig. 4A, blue cluster). The rest of the clusters were more heterogenous, combining MN pools innervating antagonists. Namely, 1) finger flexors and extensors (FDP, FDS, and EDS in the magenta cluster), 2) elbow flexor and wrist extensor (BIC and ECR in the violet cluster) and 3) elbow extensor and wrist flexor (TRI and FCR in the pink cluster, Fig. 4A). The first heterogenous cluster may enable efficient coactivation of muscles stabilizing the wrist during object manipulation. The second heterogenous cluster may underlie the coactivation of elbow flexors and wrist extensors to support the arm against gravity during reaching with palm down. The third heterogenous cluster may underlie the coactivation of elbow extensors and wrist flexors to support retrieval movements that bring objects to toward the body (Graziano 2006).

Interestingly, when the rostrocaudal locations of the MN pools are excluded from the clustering analysis, the first heterogenous cluster broke apart into agonistic clusters of wrist and finger flexors (FCR, FCU, FDP, and FDS in pink cluster) and wrist and finger extensors (ECR,

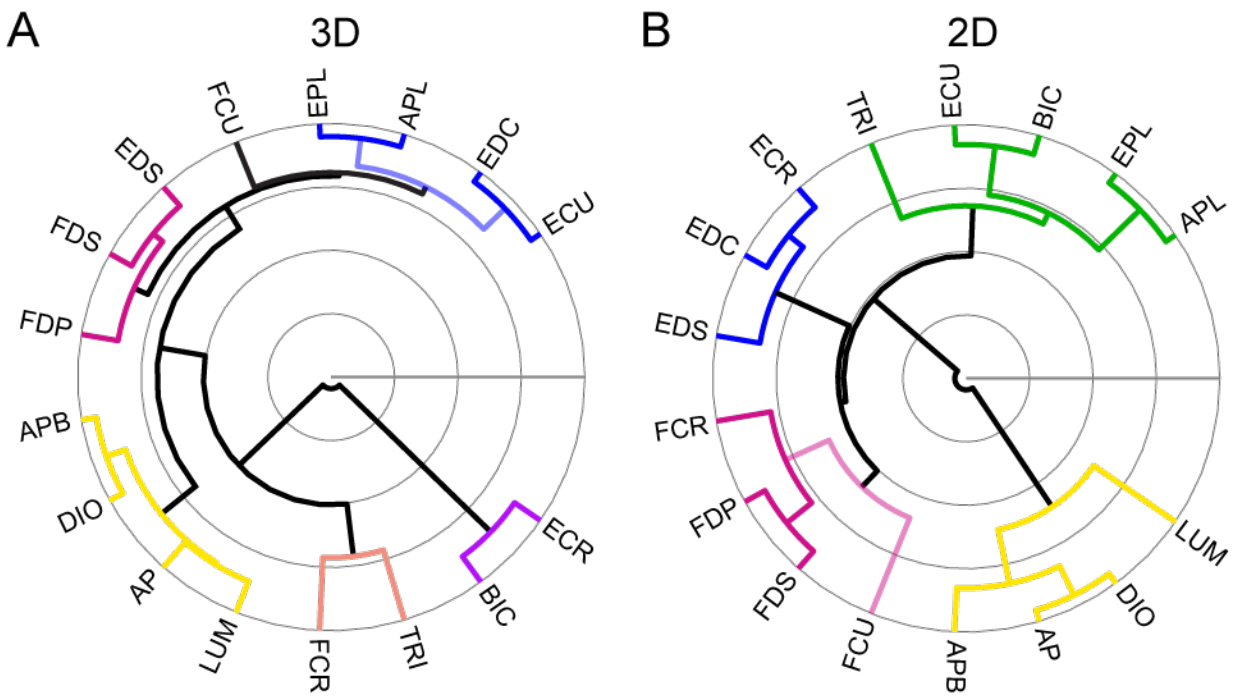

Figure 4. Hierarchical clustering of MN pools in the macaque spinal cord. Lines extending out from the center represent the relative distances between the center of mass calculated for MN pools corresponding to each muscle. Matching colors indicate the similarity of members in a given cluster in both subplots. **A.** Analysis along all 3 dimensions. Colors outline 6 clusters; transparent colors outline a further subdivision into 7 clusters. **B.** Analysis along medial/lateral and anterior/posterior dimensions only. Colors outline the 4 clusters; transparent colors outline a further subdivision into 5 clusters.

EDS, and EDC in blue cluster, Fig. 4B). The agonistic cluster of MN pools innervating some thumb muscles and intrinsic hand muscles remained the same (yellow cluster), while the remaining heterogenous cluster acquired bicep and triceps MN pools, while losing EDC MN pool to the agonistic extensor cluster (Fig. 4B, green cluster). These changes were driven by the large differences in rostrocaudal locations of the proximal muscles that changed cluster allocations, such as BIC, TRI, ECR, and FCR, from the rest of the muscles (Fig. 3). This shows that the proximity of MN pools innervating antagonists along the rostrocaudal direction of the spinal cord suggests congruency with the distribution of descending and propriospinal inputs across multiple segments, which are important for co-contraction of antagonistic muscles and underlies the neural control of complex actions. In contrast, the proximity of MN pools innervating agonists along the mediolateral and anterior/posterior directions of the spinal cord, i.e., within the segmental planes, suggest congruency with the distribution of afferent inputs and local interneurons within the same segment, circuitry that underlies coactivation of agonistic muscles.

<u>Neural embedding of muscle function in macaque</u>

Could the anatomical locations of MN pools have functional significance? To answer this question, we compared the relationships between the MN pool locations in the spinal cord to the functional relationships between muscles they innervate. The functional relationships between the

muscles were obtained by analyzing the changes in muscle lengths across the whole repertoire of arm postures simulated in an OpenSim model of the macaque upper extremity. Only muscles for which MN data was included in our spinal cord model were included in the muscle lengths analysis. Changes in muscle lengths are positively correlated for muscles performing similar actions and negatively correlated for those performing antagonistic actions (Fig. 5A). Hierarchical cluster analysis has shown that the flexor muscles largely change length together and the extensors and thumb abductors largely change length together (Fig. 5B). These relationships were broadly similar to those based on the anatomical distribution of the MN pools, particularly in the segmental plane (Fig. 4B).

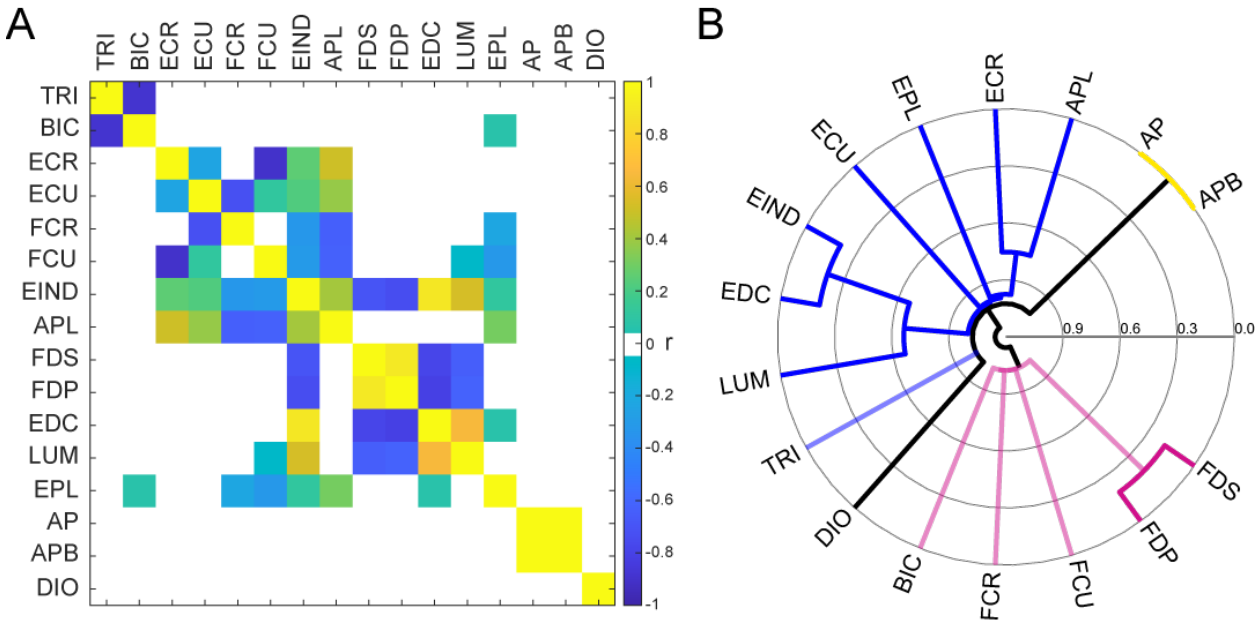

Figure 5. Functional muscle anatomy evaluated across the full range of motion of the macaque forelimb. **A.** Correlation matrix of Pearson correlation coefficients (r) between muscle lengths of all muscle pairs. The correlation matrix of muscle lengths across all postures was converted to heterogeneous variance explained (HVE) to emphasize agonistic relationships and hierarchical clustering was then applied to the HVE. B. Hierarchical clustering of the HVE based on the correlation matrix in A. Colors outline 4 clusters, transparent colors outline the further subdivisions into up to 8 clusters. Matching colors indicate the similarity of members in a given cluster to those in Fig. 4.

To quantitatively assess the similarity between the anatomical distribution of MN pools and the functional relationships based on muscle lengths, we used the Fowlkes-Mallow index (B_k) as described in Methods. To assess the likelihood that the similarities between these relationships were due to chance, we compared B_k values to those calculated from randomly permuted cluster assignments. This analysis has shown that the anatomical relationships between MN pools across all dimensions of the spinal cord were most similar to those based on muscle lengths at six- and seven-cluster subdivision (B_k = 0.43 & 0.41; p = 0.002 & < 0.007, respectively; Fig. 6A). These cluster subdivisions are highlighted in colors in figure 4A identifying the synergistic and

heterogeneous clusters described above. For clustering along the segmental plane, the four- and five-cluster subdivisions were most similar across anatomical and functional relationships (B_k = 0.47 & 0.46, p = 0.003 & 0.001, respectively; Fig. 6B). These cluster subdivisions are highlighted in colors in figure 4B identifying primarily the synergistic clusters described above. This quantitatively supports the conclusions above regarding the anatomical distribution of the MN pools underlying the synergistic and antagonistic actions of muscles they innervate.

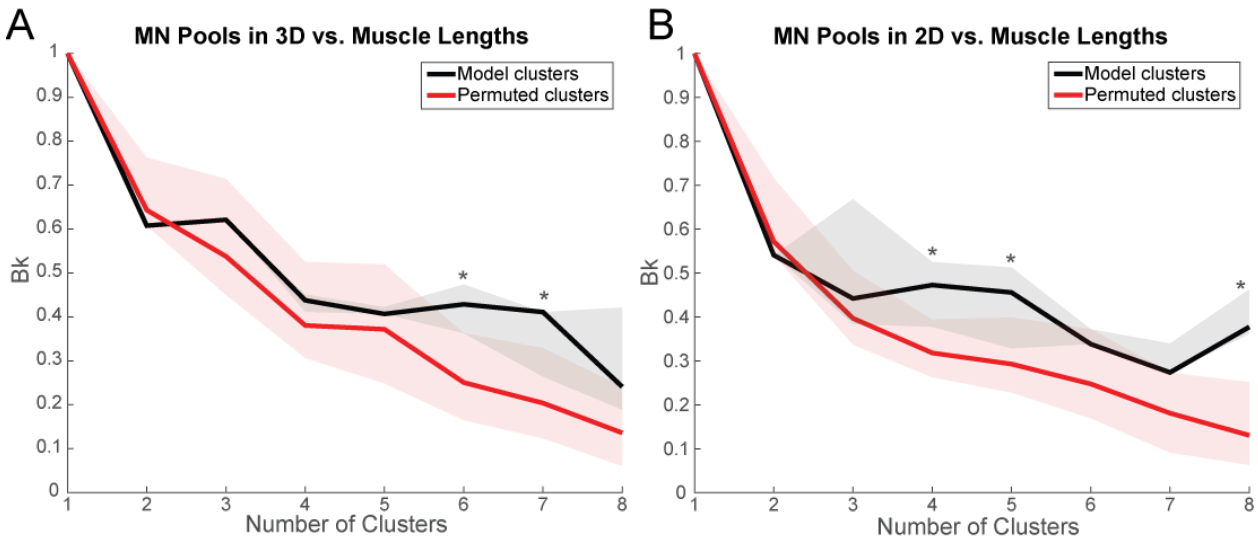

Figure 6. The similarity between clustering of spinal MN pool locations and muscle lengths. Lines show the Fowlkes-Mallow Index (B_k) that quantifies the levels of similarities between clusters of distances between centers of MN pools in the macaque spinal cord model and clusters of changes in muscle lengths derived from the OpenSim model. Black lines show B_k values from the model comparisons and the grey shaded area shows the variability of clusters obtained using bootstrapping. Red lines show median values of B_k and red shaded area shows the 5th to 95th percentile of B_k values based on randomly permuted cluster assignments. **A.** Clustering of MN pools in all 3 dimensions compared to muscle lengths. **B.** Clustering of MN pools in medial/lateral and anterior/posterior dimensions only (segmental plane) compared to muscle lengths. * p < 0.007

<u>Comparative muscle anatomy of the macaque and human</u>

How similar are the functional relationships between muscles in the macaque and human? To answer this question, we compared the relationships between muscle lengths across the full range of postures obtained from human and macaque OpenSim models (Fig. 2). These OpenSim models allowed us to analyze the functional relationships underlying the synergistic and antagonistic actions of multiple muscles of the whole upper extremity in both human and macaque. Muscle lengths were found to be changing together reflecting their functional actions, broadly forming similar groups in both models. For example, the lengths of wrist and finger extensors changed together across postures (Fig. 7, blue clusters) in a synergistic manner with elbow flexors and forearm supinators (Fig. 7, green clusters) and in an antagonistic manner with finger flexors (Fig. 7, pink clusters). Similarly, the lengths of wrist and finger flexors changed in a synergistic manner with that for elbow extensors (Fig. 7, orange cluster). The only pronounced difference

between species was in the functional grouping of APL. In the macaque, this thumb abductor muscle groups most closely with wrist extensors (ECR_L and ECR_B) and other finger extensors (Fig. 7A, green cluster) likely to enable hand opening with wrist extension moment necessary to support the pronated hand against gravity. However, in the human APL groups with EPB (Fig. 7B), potentially enabling the independent extension and abduction of the thumb, e.g., thumbs up gesture. Interestingly, the MN pool for APL is one of the few MN pools that are distributed differently along the rostrocaudal direction of the spinal cord in the macaque and human (Fig. 3). Overall, the vast majority of upper limb muscles showed very similar functional relationships in both the macaque and human. These similarities suggest that the neural embedding of muscle function in macaque spinal cord is likely representative of the neural embedding of muscle function in the human spinal cord.

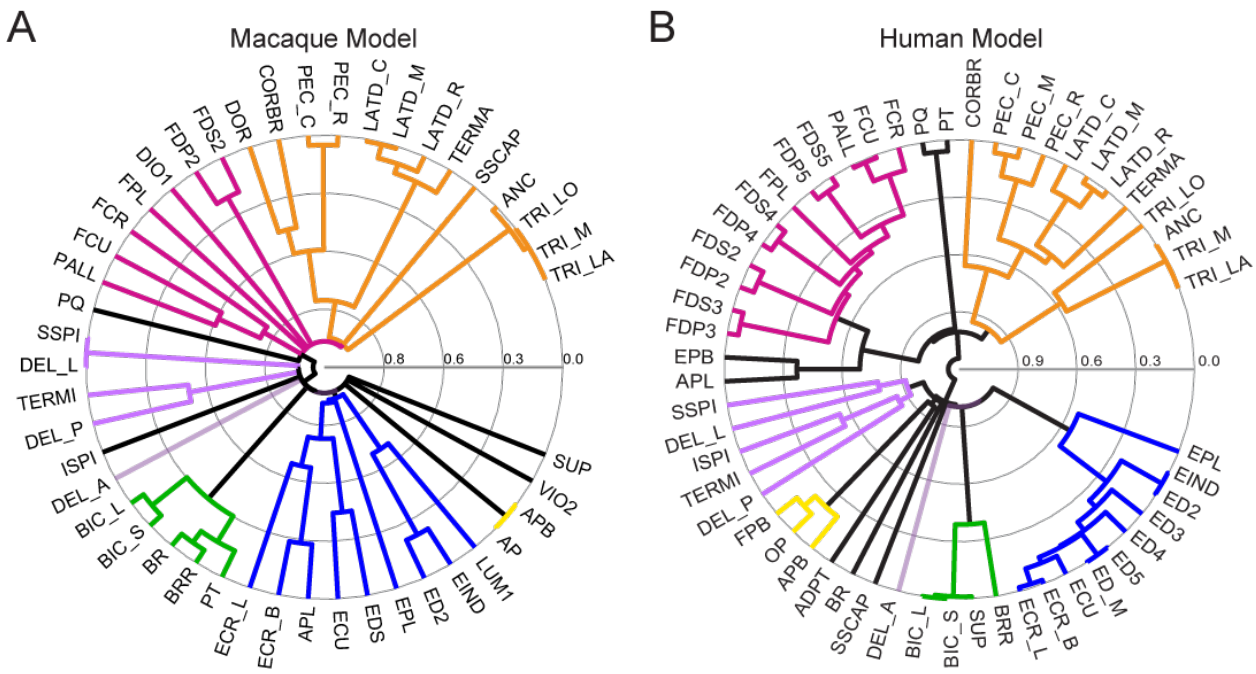

Figure 7. Functional relationships between muscles in the macaque and human. Hierarchical clustering of changes in muscle lengths across the full range of upper limp postures derived from both the macaque and human OpenSim upper extremity models. **A.** and **B.** Lines emanating from the centers of the polar dendrograms indicate the distance between muscle clusters calculated from HVE (see Methods). The similar clusters are highlighted in matching colors.

Discussion

In this study, we have created the first three-dimensional model of select spinal MNs innervating skeletal muscles of the upper extremity in the macaque. Using this model, we have shown that the MN pools innervating 16 upper limb muscles in macaque are located in similar segments as their human counterparts (Fig. 3). We have also shown that the functional relationships between muscles that these and other MN pools innervate are also very similar

between macaque and human upper limbs (Fig. 7). These results highlight the similarity of anatomy of these two species. We further found that, within the same segment, the MNs innervating synergistic muscles were located closer to each other than to the MNs innervating antagonistic muscles, while across segments MNs innervating specific antagonistic groups of muscles were located closer together in the spinal cord. These spatial relationships were similar to the functional relationships between muscles derived from muscle length changes across multiple arm postures (Fig. 4 and 5). This suggests that the anatomical distribution of the MN pools underlies the synergistic and antagonistic actions of muscles they innervate, providing evidence for the neural embedding of muscle function in spinal cord anatomy.

Our 2D analysis of the MN locations within the corresponding segments have shown that the MNs grouped primarily according to the synergistic actions of the muscles they innervate. Specifically, one cluster comprised MN pools innervating muscles involved in the extension and abduction of fingers 2-5 and the abduction and flexion of the thumb (Fig. 4B, yellow cluster), i.e., hand opening for object grasping. Another cluster comprised MN pools innervating muscles involved in the extension of all fingers but the thumb (Fig. 4B, blue cluster), while another cluster comprised MN pools innervating muscles involved in the flexion of wrist and all fingers except the thumb (Fig. 4B, red). The last cluster was more heterogeneous comprising MN pools innervating muscles involved in thumb abduction with extension, wrist extension, elbow flexion, and, less closely related, elbow extension (Fig. 4B, green cluster), potentially underlying the action of holding the hand palm down with elbow flexed against gravity. This anatomical arrangement of MN pools may be useful for transmitting the afferent feedback from the muscle spindles and tendon organs to the heterogenous MNs innervating agonists forming reflex arcs that reinforce coactivation of agonistic muscles. Such afferent-driven muscle activity has been shown for hindlimb extensor muscles in the cat during the stance phase of walking (Hiebert and Pearson 1999; Prochazka et al. 1997a) and it likely underlies positive force feedback control and other similar types of muscle coactivation in humans (Hagbarth 1993; Prochazka et al. 1997b). The afferent-driven coactivation of synergistic upper limb muscles during reaching in humans has also been suggested by simulations of primary afferent feedback and their relationships to muscle activation patterns (Hardesty et al. 2020).

Considering the rostrocaudal distribution of MN pools reveals the proximity of heterogenous MN pools innervating antagonists. One such cluster comprised MN pools innervating muscles involved in both flexion and extension of all fingers except the thumb (Fig. 4A, magenta cluster). Another cluster comprised MN pools innervating muscles involved in the flexion and extension of the wrist, extension of the fingers, and abduction of the thumb (Fig. 4A, blue cluster with FCU included). Such rostrocaudal proximity of MN pools innervating antagonistic muscles may be useful for supporting their co-contraction and increasing the stiffness of the wrist during arm motion and object manipulation. The joint stiffness is a component of joint impedance (Hogan 1985). The joint and, possibly, whole arm impedance is thought to be a controlled parameter in the central nervous system (Franklin et al. 2007; Milner and Franklin 2005). It has been shown that impedance varies with the stability of movement, i.e., higher

impedance occurs when movement stability is challenged (Burdet et al. 2001; Milner 2002a; Rancourt and Hogan 2001). The amount of muscle co-activation increases in movements with unstable loads compared to those with stable loads (Milner 2002b). The impedance of the whole limb has also been shown to stabilize movement in novel dynamical tasks (Milner and Franklin 2005). The joint stiffness component of impedance has been shown to be higher during unconstrained movements compared to constrained ones indicating, unsurprisingly, that unconstrained movements are inherently less stable (Damm and McIntyre 2008). Wrist stiffness increases during unstable dynamical loads compared to stable ones (De Serres and Milner 1991) and when the accuracy demands of the task are higher (Wong et al. 2009). Our results indicate that the spinal embedding of muscle dynamics may underlie the neural control of impedance.

The rostrocaudal distribution of MN pools also reveals the proximity of MN pools innervating antagonistic muscles spanning different joints, such as those involved in elbow flexion with wrist extension and in the opposite action of elbow extension with wrist flexion (Fig. 4A, violet and pink clusters respectively). These clusters may enable synergistic activation of elbow flexors and wrist extensors to support the arm against gravity during reaching with palm down and the activation of elbow extensors and wrist flexors to support retrieval movements that bring objects toward the body. Similar actions have been evoked by motor cortical stimulation in monkeys (Graziano 2006) and are thought to represent the modular organization of the hierarchal neural control schema (Mussa-Ivaldi 1999; Ting et al. 2015; Tresch et al. 2002).

References

Angelaki DE, **Shaikh AG**, **Green AM**, **Dickman JD**. Neurons compute internal models of the physical laws of motion. *Nature* 430: 560–564, 2004.

d'Avella A, **Saltiel P**, **Bizzi E**. Combinations of muscle synergies in the construction of a natural motor behavior. *Nat Neurosci* 6: 300–308, 2003.

Bernstein N. Physiology of movement and activity. *Nauka* 373–392, 1990.

Berringer OR, **Browning FM**, **Schroeder CR**. *An Atlas and Dissection Manual of Rhesus Monkey Anatomy.* Florida State University, Tallahassee: Anatomy Laboratory Aids, 1968.

Bizzi E, **Cheung VC**. The neural origin of muscle synergies [Online]. *Frontiers in Computational Neuroscience* 7, 2013https://www.frontiersin.org/article/10.3389/fncom.2013.00051 [17 Jun. 2022].

Burdet E, **Osu R**, **Franklin DW**, **Milner TE**, **Kawato M**. The central nervous system stabilizes unstable dynamics by learning optimal impedance. *Nature* 414: 446–449, 2001.

Chan SS, **Moran DW**. Computational model of a primate arm: from hand position to joint angles, joint torques and muscle forces. *J Neural Eng* 3: 327–337, 2006.

Damm L, **McIntyre J**. Physiological Basis of Limb-Impedance Modulation During Free and Constrained Movements. *Journal of Neurophysiology* 100: 2577–2588, 2008.

De Serres SJ, **Milner TE**. Wrist muscle activation patterns and stiffness associated with stable and unstable mechanical loads. *Exp Brain Res* 86: 451–458, 1991.

Efron B, **Tibshirani RJ**. An Introduction to the Bootstrap [Online]. 1st ed. Chapman and Hall/CRC.https://www.crcpress.com/An-Introduction-to-the-Bootstrap/Efron-Tibshirani/p/book/9780412042317 [2 Jan. 2020].

Fowlkes EB, **Mallows CL**. A Method for Comparing Two Hierarchical Clusterings. *Journal of the American Statistical Association* 78: 553–569, 1983.

Franklin DW, **Liaw G**, **Milner TE**, **Osu R**, **Burdet E**, **Kawato M**. Endpoint Stiffness of the Arm Is Directionally Tuned to Instability in the Environment. *Journal of Neuroscience* 27: 7705–7716, 2007.

Graziano M. THE ORGANIZATION OF BEHAVIORAL REPERTOIRE IN MOTOR CORTEX. *Annu Rev Neurosci* 29: 105–134, 2006.

Gritsenko V, **Hardesty RL**, **Boots MT**, **Yakovenko S**. Biomechanical Constraints Underlying Motor Primitives Derived from the Musculoskeletal Anatomy of the Human Arm. *PLoS ONE* 11: e0164050, 2016.

Hagbarth KE. Microneurography and applications to issues of motor control: Fifth Annual Stuart Reiner Memorial Lecture. *Muscle Nerve* 16: 693–705, 1993.

Hardesty RL, **Boots MT**, **Yakovenko S**, **Gritsenko V**. Computational evidence for nonlinear feedforward modulation of fusimotor drive to antagonistic co-contracting muscles. *Sci Rep* 10: 10625, 2020.

Hiebert GW, **Pearson KG**. Contribution of Sensory Feedback to the Generation of Extensor Activity During Walking in the Decerebrate Cat. *Journal of Neurophysiology* 81: 758–770, 1999.

Hogan N. The mechanics of multi-joint posture and movement control. *Biological Cybernetics* 52: 315–331, 1985.

Jenny AB, **Inukai J**. Principles of motor organization of the monkey cervical spinal cord. *J Neurosci* 3: 567–575, 1983.

Kawato M. Internal models for motor control and trajectory planning. *Current Opinion in Neurobiology* 9: 718–727, 1999.

Kendall FP, **McCreary EK**, **Provance PG**. *Muscles, Testing and Function: With Posture and Pain*. Williams & Wilkins, 1993.

McNamee D, **Wolpert DM**. Internal Models in Biological Control. *Annu Rev Control Robot Auton Syst* 2: 339–364, 2019.

Milner TE. Adaptation to destabilizing dynamics by means of muscle cocontraction. *Experimental Brain Research* , 2002a. doi:10.1007/s00221-002-1001-4.

Milner TE. Adaptation to destabilizing dynamics by means of muscle cocontraction. *Exp Brain Res* 143: 406–416, 2002b.

Milner TE, **Franklin DW**. Impedance control and internal model use during the initial stage of adaptation to novel dynamics in humans: Initial stage of motor adaptation. *The Journal of Physiology* 567: 651–664, 2005.

Mussa-Ivaldi FA. Modular features of motor control and learning. *Current Opinion in Neurobiology* 9: 713–717, 1999.

Prochazka A, **Gillard D**, **Bennett DJ**. Implications of Positive Feedback in the Control of Movement. *Journal of Neurophysiology* 77: 3237–3251, 1997a.

Prochazka A, **Gillard D**, **Bennett DJ**. Positive Force Feedback Control of Muscles. *Journal of Neurophysiology* 77: 3226–3236, 1997b.

Rancourt D, **Hogan N**. Stability in force-production tasks. *Journal of Motor Behavior* , 2001. doi:10.1080/00222890109603150.

Saul KR, **Hu X**, **Goehler CM**, **Vidt ME**, **Daly M**, **Velisar A**, **Murray WM**. Benchmarking of dynamic simulation predictions in two software platforms using an upper limb musculoskeletal model. *Computer Methods in Biomechanics and Biomedical Engineering* 18: 1445–1458, 2015.

Ting LH, **Chiel HJ**, **Trumbower RD**, **Allen JL**, **McKay JL**, **Hackney ME**, **Kesar TM**. Neuromechanical Principles Underlying Movement Modularity and Their Implications for Rehabilitation. *Neuron* 86: 38–54, 2015.

Tresch MC, **Saltiel P**, **d'Avella A**, **Bizzi E**. Coordination and localization in spinal motor systems. *Brain Research Reviews* 40: 66–79, 2002.

Watson C, **Sengul G**, **Paxinos G**. *The Mammalian Spinal Cord*. 1st edition. Academic Press, 2022.

Wolpert DM. The real reason for brains [Online]. https://www.ted.com/talks/daniel_wolpert_the_real_reason_for_brains.

Wong J, **Wilson ET**, **Malfait N**, **Gribble PL**. Limb Stiffness Is Modulated With Spatial Accuracy Requirements During Movement in the Absence of Destabilizing Forces. *Journal of Neurophysiology* 101: 1542–1549, 2009.

Yakovenko S, **Mushahwar V**, **VanderHorst V**, **Holstege G**, **Prochazka A**. Spatiotemporal Activation of Lumbosacral Motoneurons in the Locomotor Step Cycle. *Journal of Neurophysiology* 87: 1542–1553, 2002.